1-1-2003

Three-Dimensional Reconstruction Algorithm for a Reverse-Geometry Volumetric CT System With a Large-Array Scanned Source

Taly Gilat Schmidt
Marquette University, tal.gilat-schmidt@marquette.edu

Rebecca Fahrig
Stanford University

Norbert J. Pelc
Stanford University

Three-dimensional reconstruction algorithm for a reverse geometry volumetric CT system with a large array scanned source

Taly Gilat[a,b], Rebecca Fahrig[a], Norbert J. Pelc[a]

[a] Department of Radiology, Stanford University, Stanford, CA 94305
[b] Department of Electrical Engineering, Stanford University, Stanford, CA 94305

ABSTRACT

We have proposed a CT system design to rapidly produce volumetric images with negligible cone beam artifacts. The investigated system uses a large array scanned source with a smaller array of fast detectors. The x-ray source is electronically steered across a 2D target every few milliseconds as the system rotates. The proposed reconstruction algorithm for this system is a modified 3D filtered backprojection method. The data are rebinned into 2D parallel ray projections, most of which are tilted with respect to the axis of rotation. Each projection is filtered with a 2D kernel and backprojected onto the desired image matrix. To ensure adequate spatial resolution and low artifact level, we rebin the data onto an array that has sufficiently fine spatial and angular sampling. Due to finite sampling in the real system, some of the rebinned projections will be sparse, but we hypothesize that the large number of views will compensate for the data missing in a particular view. Preliminary results using simulated data with the expected discrete sampling of the source and detector arrays suggest that high resolution (<0.5 mm in all directions) images can be obtained in a single rotation with the proposed system and reconstruction algorithm.

Keywords: computed tomography (CT), volumetric CT, 3D reconstruction

1. INTRODUCTION

Faster scan times, large anatomic coverage with thin slices, and reduced motion artifacts have been made possible by the development of multidetector computed tomography (MDCT) systems. The volume covered by current multidetector scanners is still relatively small, for example these systems require many gantry rotations to acquire the full heart volume. One logical extension of this approach is a system capable of imaging the entire volume in a single rotation, volumetric CT (VCT). As the acquired volume thickness increases, by increasing the number of detector rows or by using flat-panel digital x-ray detectors, so does the divergence angle of the x-ray cone beam in the axial direction. The problem with VCT systems with a single circular orbit is that the acquired cone-beam data set is not sufficient for an exact reconstruction.[1] For small cone angles the resulting artifacts are tolerable, but as the volume thickness increases, so does the severity of the artifacts.

We have proposed a VCT system that uses a large array scanned source and a smaller array of fast detectors. In principle, the data set acquired by this reverse geometry system should be sufficient to prevent cone-beam artifacts, as the source and detector arrays have the same axial extent.

The goal of this paper is to describe the proposed reconstruction algorithm for this system. The theoretical details of the algorithm will be presented, as well as the preliminary results.

2. PROPOSED SYSTEM GEOMETRY

The system we are proposing to acquire a sufficient VCT data set is a reverse geometry system with a large array scanned source and a smaller array of detectors. The basic system geometry is illustrated in Fig. 1.

The system is conceptually similar to that used by NexRay, Inc. for their interventional cardiology C-arm system.[2] The proposed x-ray source has an electron beam that is electromagnetically steered across a transmission target. An array of collimator holes limits the resulting small area x-ray beam so it is aimed towards the detector. The detector is comprised of a smaller array of fast photon counting detectors. During

Medical Imaging 2003: Physics of Medical Imaging, M. J. Yaffe, L. E. Antonuk,
Editors, Proceedings of SPIE Vol. 5030 (2003) © 2003 SPIE · 1605-7422/03/$15.00

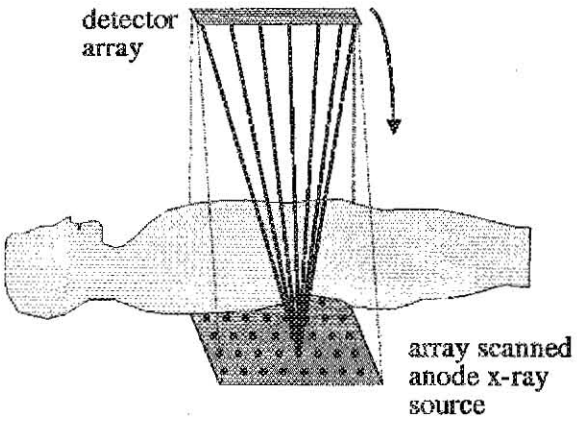

Figure 1. Proposed system geometry showing the x-ray beam at one collimator position.

an acquisition, the x-ray beam dwells on each source position (i.e., adjacent to each collimator hole) and then is steered to the next source position in the array. For each source position, the entire detector array is read out producing a 2D divergent projection covering a fraction of the field of view.

In order to use these components in a CT system, the source and detector would be mounted on a gantry and rotated around the patient.

The specifications for the preliminary CT geometry are summarized in Table 1.

Table 1. Specifications for proposed VCT geometry

Source dimensions (transverse x axial)	50 cm x 15 cm
Number of source locations	200 x 60 spots
Detector dimensions (transverse x axial)	5 cm x 15 cm
Number of detector locations	48 x 144 elements
Dwell time per source location	1 μs
Move time between successive source locations	0.28 μs

3. RECONSTRUCTION ALGORITHM

The proposed 3D reconstruction algorithm can be broken down into a rebinning step followed by filtered backprojection. The basic idea of the algorithm is to view the data not as they are acquired, but instead as a set of 2D parallel ray projections. Among the acquired rays are a set of parallel rays that are perpendicular to the axis of rotation. These "in-plane" rays are equivalent to those collected in a normal CT scan. In addition to these in-plane rays, the acquired data set also contains cross plane rays that are tilted with respect to the axis of rotation. This concept is illustrated in Fig. 2. The reconstruction algorithm first rebins the acquired data into a set of 2D parallel ray projections at numerous tilt angles, and then uses these 2D projections to reconstruct a volume. Because the source and detector sampling is finite, some of these rebinned projections may be sparse. However, because of the large number sampled views, we hypothesize that missing data in one view can be compensated by nearby projections.

This reconstruction scheme is motivated by the Fourier domain interpretation of 2D parallel ray projections. This analysis, based on the Central Slice Theorem, will be described in the filtered backprojection section. It

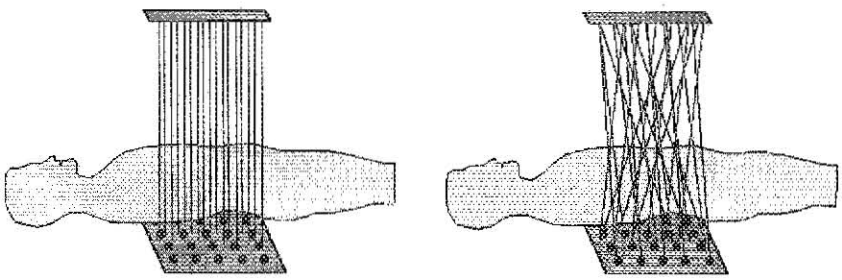

(a) An in-plane parallel ray projection

(b) Cross-plane rays

Figure 2. Rebinning acquired data into 2D parallel ray projections.

should also be noted that the rebinned data set resembles the data acquired in multi-ring Positron Emission Tomography (PET). Therefore, techniques already developed for PET reconstruction can be utilized.

The following sections describe the theory involved in the two steps of the proposed reconstruction method, and also discuss the preliminary implementation.

3.1. Rebinning algorithm

Each ray from a source location to a detector location is described by four parameters, the rotation angle, ϕ, the colatitude or tilt angle (the angle from the axis of rotation), θ, and two distance measures, ρ_{ip} and ρ_{op}, describing the location of the line from the central ray. These parameters are illustrated in Fig. 3. The two distance parameters could be combined into one distance parameter, but are kept separate in this discussion.

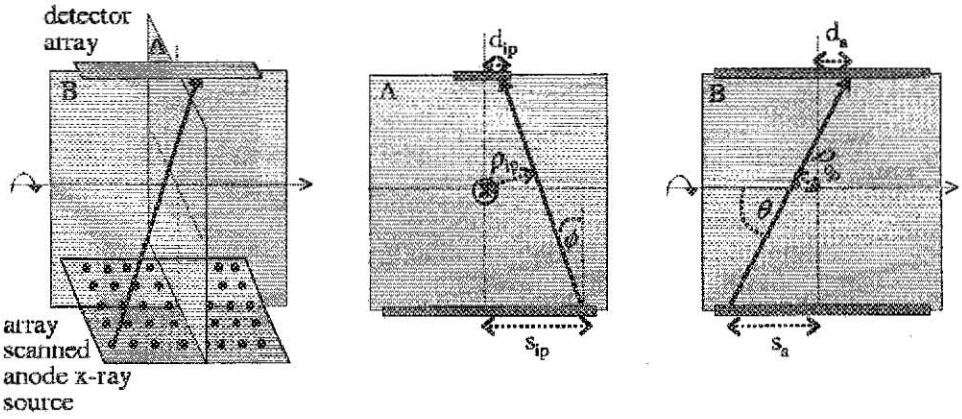

(a) A ray from the source to the detector.

(b) The projection of the ray onto plane A.

(c) The projection of the ray onto plane B.

Figure 3. Determining the four geometry parameters describing a ray in 3D space.

The four parameters can be determined geometrically. The rotation angle, ϕ, and in-plane distance, ρ_{ip},

depend on the in-plane source location, s_{ip}, and detector location, d_{ip}. As illustrated in Fig. 3(b), these two parameters can be found using the following equations.

$$\psi = \arctan\left(\frac{s_{ip} - d_{ip}}{SDD}\right) \tag{1}$$

$$\phi = \psi + \phi_{gantry} \tag{2}$$

where ψ is the rotation angle of the ray without gantry rotation, and SDD is the source to detector distance. To find the total rotation, the gantry rotation, ϕ_{gantry} is added to ψ as shown in Eq. 2. The in-plane distance is

$$\rho_{ip} = d_{ip} * \cos(\psi) + DID * \sin(\psi) \tag{3}$$

where DID is the detector to isocenter distance. As shown in Eq. 3, ρ_{ip} is independent of gantry rotation.

Similarly, θ and ρ_{op} depend on the axial source and detector positions, s_a and d_a respectively as shown in Fig. 3(c), and can be calculated using the following equations.

$$\theta = \frac{\pi}{2} - \arctan\left(\frac{s_a - d_a}{SDD}\right) \tag{4}$$

$$\rho_{op} = d_a * \sin(\theta) + DID * \cos(\theta) \tag{5}$$

The goal of the rebinning algorithm is to take each ray and place it into a 2D parallel ray projection. The two angle parameters, ϕ and θ, determine the gantry rotation angle and the gantry tilt angle of the corresponding projection, and the two distance parameters determine the ray's location within the projection. Therefore, these four parameters are sufficient for reorganizing the data into 2D parallel ray projections. However, in a discrete implementation with a reasonable number of projections, especially projections that are equally spaced in each of the four parameters, nearby rays must be binned together using some form of interpolation or gridding.

To better understand the rebinning algorithm, it is useful to visualize the data in Radon space. For 2D reconstruction with 1D projections, such as those acquired by conventional single slice CT systems, each acquired ray can be described by two parameters, the projection angle ϕ and the perpendicular distance of the ray to the axis of rotation, ρ. For single slice CT systems, Radon space is two dimensional, with ρ and ϕ as the two coordinate axes. Therefore, each ray acquired in a 1D projection samples one point in the two dimensional Radon space. Each parallel projection samples one horizontal line in 2D Radon space. In a single slice fan-beam system, each fan-beam samples a tilted line in Radon space.

For our proposed system geometry, each ray is described by two angles and two distances, and thus is represented by a four dimensional Radon space. Each ray samples one point in 4D Radon space, but the sample points from all the input rays are not distributed evenly. The rebinning algorithm must convert the nonuniformly sampled 4D Radon space data into uniformly spaced samples

The problem of resampling nonuniform data onto a uniform grid has come up in many different fields, and much work has been done to solve it. We are using the gridding approach.[3]

The first step in the gridding algorithm is to determine a bin width or kernel width for each of the four geometry parameters. Our current implementation is output-grid-driven. That is, for each output grid point in our uniformly spaced 4D Radon space, the algorithm finds the input data points that fall within the 4D bin. Each input data point is weighted based on its distance to the grid point, where the weight is determined by a chosen 4D kernel shape. At the output grid point, the weighted values of all the contributing data points are accumulated as are the sum of all the weights.

One important step in the rebinning algorithm is to compensate for the nonuniform sampling density of the original data points. This can be done by pre-weighting the data according to the sampling density of the input data points, by post-weighting the output data based on the total deposited weights at each grid point,

or by using a combination of both methods. In our preliminary implementation, we are using post-weighting compensation and have also been investigating more accurate pre-weighting methods.

The important design parameters in the gridding algorithm are the bin widths, kernel shape, and output grid sampling density. For application in MRI reconstruction, the effect of each of these parameters on the rebinned data has been described in detail.[4] For the preliminary VCT implementation of this algorithm, these parameters were chosen experimentally. For computational simplicity, the 4D kernel was designed as four separable Hanning window kernels in each dimension. The output grid spacing was chosen as the largest spacing that provided acceptably low artifacts. The bin widths were chosen to trade off the blurring caused by large bin widths while reducing the occurrence of empty output grid points which are caused by small bin widths.

3.2. Filtered backprojection

The key to accurate reconstruction for filtered backprojection is in the filter design. In the spatial domain, the filtering step can be seen as correcting the impulse response of the backprojection process. That is, the generally negative tails of the reconstruction kernel exactly cancel the positive tails (blurring) that results if a band limited impulse is backprojected.

Having the data organized into 2D parallel ray projections provides a useful method for designing the filter in Fourier space using the Central Slice Theorem, which states that a 2D parallel ray projection of a 3D object samples the Fourier transform of the object along the plane perpendicular to the projection direction. So as numerous 2D projections are acquired, the Fourier transform of the object is sampled along the corresponding planes. As a result, 3D frequency space is not sampled uniformly, with certain regions sampled more than others. It can also be shown that the Fourier transform of the backprojection of a single 2D projection into a 3D volume is non-zero only on the same plane that was sampled by that projection.[5]

The role of the reconstruction filters is to weight the frequency content of each projection so that, when they are all superimposed, the 3D Fourier transform of the object is properly reconstructed. In our approach, the filter applied to each projection is the inverse of the density of measurements in frequency space on the plane sampled by that projection.

An analytical solution for this filter has been derived for 2D parallel ray projections equally spaced over a range of tilt angles[6] and will be stated without proof below.

The 2D filter for a 2D parallel ray projection at a colatitude angle θ is

$$G_\theta(k_u, k_v) = \frac{W(k)}{D_\theta(k, \alpha)} \tag{6}$$

where k_u and k_v are the coordinates of the 2D Fourier transform of the projection, we define

$$k = \sqrt{k_u^2 + k_v^2} \tag{7}$$

$$\alpha = \arccos\left(\frac{k_v \sin\theta}{k}\right) \tag{8}$$

and W(k) is a window function used to control the impulse response. D_θ is the density of measurements on the plane in frequency space that is sampled by the projection. For our case, we assume that the projections are continuously and uniformly distributed between ϕ equal to zero and 2π and colatitude angle between θ_{min} and $\pi/2$, where θ_{min} is the colatitude angle of the most oblique projection. This is a reasonable assumption if the distance between adjacent projections is small in both angular directions. The resulting D_θ, without proof, is

$$D_\theta(k, \alpha) = \frac{M \arcsin\left(\frac{\cos(\theta')}{\sin(\alpha)}\right)}{\pi k \cos(\theta_{min})} \tag{9}$$

where M is the total number of projections and θ' is defined as

$$\theta' = \max\left(\theta_{min}, \frac{\pi}{2} - \alpha\right) \tag{10}$$

Using the expression for D_θ, we can write the equation for the 2D filter as

$$G_\theta(k_u, k_v) = \frac{\pi k \cos(\theta_{min})}{M \arcsin(\frac{\cos(\theta')}{\sin(\alpha)})} * W(k) \tag{11}$$

As can be seen, the filter depends on the colatitude or tilt angle of a given projection, but is the same for all projections at that colatitude angle.

To summarize the filtered backprojection step, for each rebinned 2D parallel ray projection, the 2D Fourier transform is calculated. The transform is then multiplied by the 2D filter described in Eq. 11. Finally the filtered projection is three dimensionally backprojected into the output volume.

4. METHODS

The 3D filtered backprojection algorithm has been implemented for reconstructing a volume from 2D parallel ray projections at multiple tilt angles. This algorithm has been tested with simulated ideal parallel ray projections and found to have artifacts at levels below the CT noise floor.

The 4D Radon space rebinning algorithm has been implemented and is currently being tested.

To explore the image quality performance of the rebinning algorithm, a simpler 2D version was implemented to reconstruct 2D slices from the in-plane sampling of the source and detector illustrated in Fig. 4 (i.e. an in-plane geometry). This algorithm takes the rays connecting one source row to one detector row and rebins them into 1D parallel ray projections. Standard filtered backprojection is used to reconstruct the in-plane slice from these 1D projections. This in-plane reconstruction algorithm provides a method to test the in-plane resolution of the system, and also to investigate the effects of the rebinning algorithm on the output image quality.

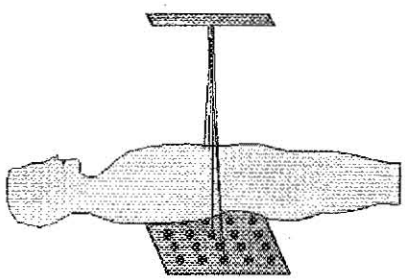

Figure 4. The in-plane sampling is the rays connecting one source row and one detector row collected during a full rotation about the object.

The following section briefly describes the results obtained using the in-plane reconstruction algorithm. The two experiments described below use the simulated in-plane sampling of the available NexRay source and detector. The simulated source row had 100 elements over 25 cm, and the simulated detector row had 48 elements over 5 cm. Seventy-one projections over a 360 degree gantry rotation (each comprised of rays connecting all source locations in one source row with all the detector elements in one detector row) were simulated with the in-plane geometry, as this number of projections was found to sufficiently sample the 2D Radon space for the field of view (FOV) used. The projections were then rebinned into 1000 parallel ray projections with an output detector pitch of 1/8 mm. For comparison, ideal 1D parallel ray projections were also generated. The ideal parallel ray projections had the same Radon space sampling as the rebinned projections. The simulated detector aperture and source focal spot blurring were kept constant for both simulations, with the focal spot modeled as a 0.8 mm by 0.8 mm rect function and the detector aperture modeled as a 1 mm by 1 mm rect function. Standard filtered backprojection was then used to reconstruct the image.

For the rebinned in-plane projections, a second reconstruction was performed where the backprojection filter was modified to undo the blurring caused by the rebinning step. The correction was based on the Fourier transform of the ρ gridding kernel. This deapodization function was thresholded so as not to greatly amplify any artifacts or noise.

In all cases, the reconstructed FOV was 7 x 7 cm with a pixel size of 1/8 x 1/8 mm.

5. RESULTS

5.1. In-plane resolution

The in-plane reconstruction algorithm has made it possible to investigate the resolution capabilities of the system. The in-plane MTF was calculated by simulating a small sphere at iso-center with radius 1/16 mm. Fig. 5 compares the MTF for the three simulated cases: the in-plane sampling, ideal parallel ray projections, and in-plane sampling with correction for the blurring from the gridding step. It is important to note that for the first two cases the backprojection filter was windowed with a Hanning window; filters with higher gain at high spatial frequencies could be used and would yield higher spatial resolution. Fig. 5 shows that slight blurring is introduced by the rebinning algorithm, but that most of this blurring can be recovered with the modified reconstruction filter. For the in-plane sampling, the 10% point is approximately 14 cm^{-1} without the deapodization, and is approximately 18 cm^{-1} with the correction.

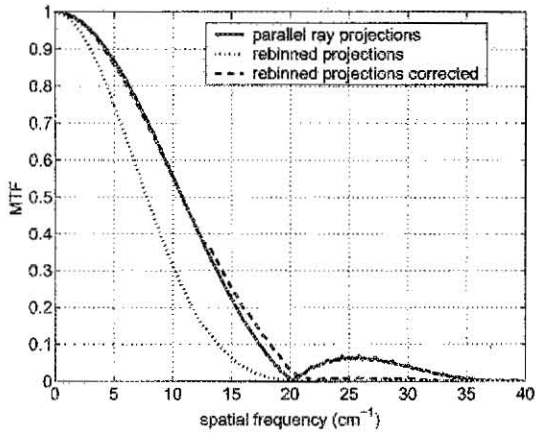

Figure 5. MTF comparison for ideal parallel ray projections, rebinned in-plane projections, and rebinned in-plane projections with corrected backprojection filter.

A resolution phantom was also simulated using small sphere objects. The resolution patterns ranged from 0.7 mm (7.1 lp/cm) in the upper right hand corner, to 0.4 mm (12.5 lp/cm) in the lower right hand corner. Fig. 6 shows the images resulting from the three reconstructions.

Comparing the images, the blurring caused by the rebinning algorithm is noticeable, but using the modified filter does improve the resolution. Looking at the corrected in-plane reconstruction, Fig. 6(c), some resolution loss can be seen towards the edge of the FOV, which is likely due to the residual blurring in the ϕ direction introduced by the rebinning algorithm. An additional deapodization step, before filtered backprojection, could be implemented to reduce this. Despite the blurring caused by the rebinning step, for all three reconstructions, the 0.4 mm pattern can be resolved.

5.2. Rebinning algorithm artifacts

To explore the accuracy of the rebinning algorithm, projections were simulated through an off-center uniform sphere of water.

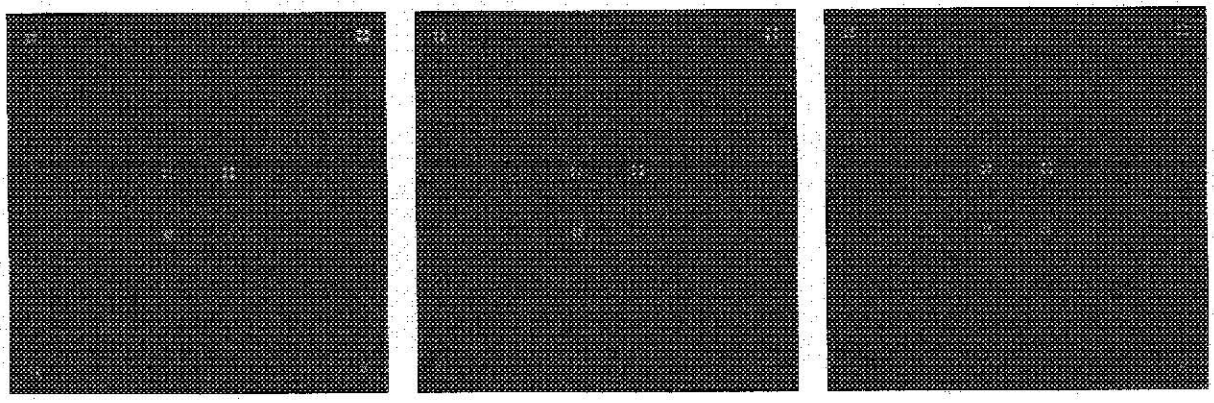

(a) in-plane sampling (b) ideal parallel ray (c) in-plane sampling with corrected backprojection filter

Figure 6. Simulated resolution phantom. Tested frequencies are, counter-clockwise from the upper right hand quadrant, 0.7 mm, 0.6 mm, 0.5 mm, 0.4 mm.

The sphere had a radius of 2.5 cm and was centered at (0.5 cm, 0.5 cm). Fig. 7 shows images reconstructed using the rebinned in-plane projections, the ideal parallel ray projections, and the rebinned in-plane rays with correction. The images are windowed to the level of 0 HU and a width of +/- 1 HU (i.e., values -1 and +1 HU are mapped to black and white, respectively). Comparing the images, the artifact level within the water sphere is similar for all images and is below 1 HU. The ideal and corrected reconstructions have ringing artifacts at the edge of the sphere that are not present in the image with the unmodified rebinned rays due to blurring introduced by the rebinning algorithm.

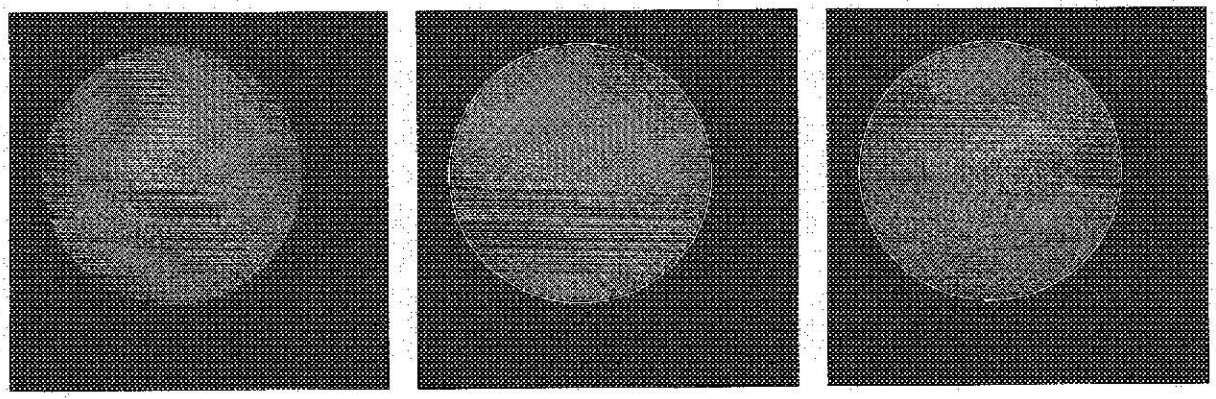

(a) in-plane sampling (b) ideal parallel ray (c) in-plane sampling with corrected backprojection filter

Figure 7. Simulated water sphere. These images were windowed to a level of 0 HU and a width of +/- 1 HU to show artifacts in the sphere.

Fig. 8 shows the three images windowed to a level of -1000 HU with a window width of +/- 1 HU to show

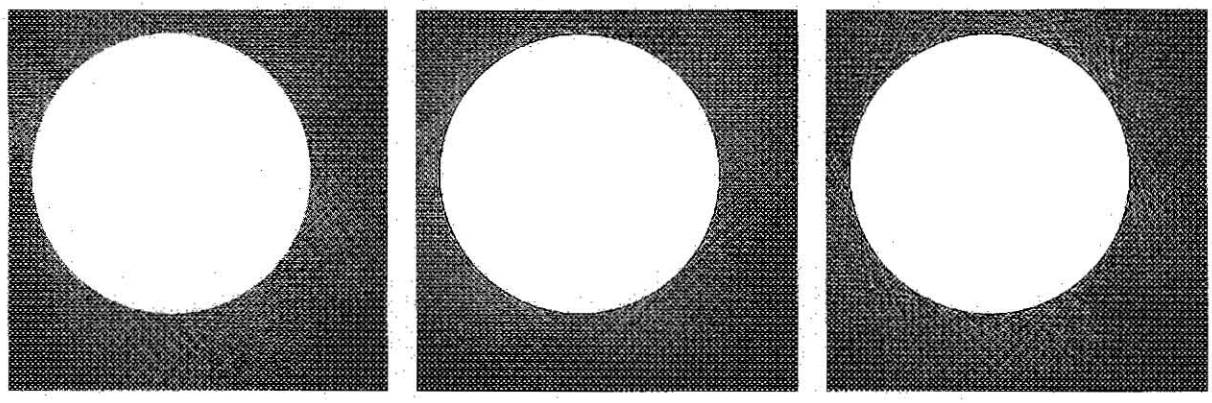

(a) in-plane sampling (b) ideal parallel ray (c) in-plane sampling with corrected backprojection filter

Figure 8. Simulated water sphere. These images were windowed to a level of -1000 HU and a width of +/- 1 HU to show artifacts outside the object

artifacts in air. The in-plane sampling has more view aliasing artifacts than the ideal parallel ray geometry, and these artifacts are amplified by the modified backprojection filter used in Fig. 8(c). Despite this amplification, the artifacts are on the order of 1 HU and thus are acceptably low.

6. CONCLUSIONS

Although the complete reconstruction algorithm has not yet been fully tested, preliminary results suggest that the proposed algorithm is feasible for the reverse geometry VCT system. Results using the in-plane reconstruction algorithm show that the rebinning step introduces no significant artifacts and only slight blurring, most of which can be recovered using a corrected reconstruction filter. Experiments using the in-plane reconstruction algorithm also demonstrate an in-plane resolution better than 0.5 mm.

ACKNOWLEDGMENTS

This work is supported by GE Medical Systems. The authors would like to thank Edward Solomon of NexRay, Inc. for helpful discussions.

REFERENCES

1. B. D. Smith, "Cone-beam tomography: recent advances and a tutorial review," *Optical Engineering* **29**, pp. 524–534, 1990.
2. E. G. Solomon, B. P. Wilfley, M. S. Van Lysel, A. W. Joseph, and J. A. Heanue, "Scanning-beam digital x-ray (SBDX) system for cardiac angiography," in *Medical Imaging 1999: Physics of Medical Imaging. Proc. SPIE* **3659**, pp. 246–257, 1999.
3. J. O'Sullivan, "A fast sinc function gridding algorithm for Fourier inversion in computer tomograpy," *IEEE Trans. Med. Imaging* **4**, pp. 200–207, 1985.
4. J. I. Jackson, C. H. Meyer, D. G. Nishimura, and A. Macovski, "Selection of a convolution function for Fourier inversion using gridding," *IEEE Trans. Med. Imaging* **10**, pp. 473–478, 1991.
5. N. J. Pelc and D. A. Chesler, "Utilization of cross-plane rays for three-dimensional reconstruction by filtered back-projection," *J. Comput. Assist. Tomogr.* **3**, pp. 385–395, 1979.
6. N. J. Pelc, "A generalized filtered backprojection algorithm for three dimensional reconstruction,". PhD dissertation, Harvard University, Boston, MA, 1979.